Received: 19 October 2022 | Accepted: 20 March 2023

DOI: 10.1002/nau.25186

BASIC SCIENCE ARTICLE

Neurourology Urodynamics | SUFU Society of Urodynamics, Female Pelvic Medicine & Urogenital Reconstruction | WILEY

Urinary flow through urethras with a rough lumen

Patricia J. Yang[1,2] | **Tony G. Chen**[1,3] | **Sarah B. Bracher**[1,4] | **Aaron Hui**[1] | **David L. Hu**[1,5]

[1]George W. Woodruff School of Mechanical Engineering, Georgia Institute of Technology, Atlanta, Georgia, USA

[2]Department of Power Mechanical Engineering, National Tsing Hua University, Hsinchu, Taiwan

[3]Department of Mechanical Engineering, Stanford University, Stanford, California, USA

[4]Medical College of Georgia, Augusta, Georgia, USA

[5]School of Biological Sciences, Georgia Institute of Technology, Atlanta, Georgia, USA

Correspondence
Patricia J. Yang and David L. Hu, George W. Woodruff School of Mechanical Engineering, Georgia Institute of Technology, Atlanta, GA 30332, USA.
Email: peijyang@pme.nthu.edu.tw and hu@me.gatech.edu

Funding information
National Science Foundation Faculty Early Career Development Program (Division of Physics), Grant/Award Number: 1255127; Ministry of Education, Taiwan; Georgia Tech Presidents Undergraduate Research Awards

Abstract

Aims: This study investigates how lumen roughness and urethral length influence urinary flow speed.

Methods: We used micro-computed tomography scans to measure the lumen roughness and dimensions for rabbits, cats, and pigs. We designed and fabricated three-dimensional-printed urethra mimics of varying roughness and length to perform flow experiments. We also developed a corresponding mathematical model to rationalize the observed flow speed.

Results: We update the previously reported relationship between body mass and urethra length and diameter, now including 41 measurements for urethra length and 10 measurements for diameter. We report the relationship between lumen diameter and roughness as a function of position down the urethra for rabbits, cats, and pigs. The time course of urinary speed from our mimics is reported, as well as the average speed as a function of urethra length.

Conclusions: Based on the behavior of our mimics, we conclude that the lumen roughness in mammals reduces flow speed by up to 25% compared to smooth urethras. Urine flows fastest when the urethra length exceeds 25 times its diameter. Longer urethras do not drain faster due to viscous effects counteracting the additional gravitational head. However, flows with our urethra mimics are still 6 times faster than those observed in nature, suggesting that further work is needed to understand flow resistance in the urethra.

KEYWORDS
major loss, roughness, urethra

1 | INTRODUCTION

While the urethra is the conduit by which urine exits the body, the resistance to flow is poorly understood. Of particular importance in flow resistance is the urethra's soft inner wall, the lumen. Characterizing the lumen is important in building more accurate models of urinary flow.[1] Such models may one day predict how micturition is influenced by trauma or disease. The goal of this study is to measure the roughness of the urethra lumen in mammals and to show how this roughness influences micturition speed. We begin by reviewing the anatomy of the urinary system, and then turn to advances in mathematical modeling of micturition.

Research on the urinary system has long neglected the urethra. The ureter, which guides urine from the bladder, attracted attention due to the medical uses of stent implants,[2] and the impact of the implant's shape

and material on the ensuing fluid dynamics. The bladder has also received attention, with a focus on its material properties, which have been measured in humans[3] and other mammals.[4] Efforts are being made to correlate the bladder's neural signal, deformation, and the pressure generated.[5,6]

The urethra connects the bladder to the outside world. The urethra of a human female has an inner diameter of only 6 mm and is connected by tissue to the reproductive tract.[7] It is soft and can only be dissected out of the body with great care. Once excised, the surface tension of water glues the lumen together like a deflated balloon. Thus, little is known about the urethra when urine flows through it. In 1972, Woodburne dissected the urethra of a dog, and his drawings suggest that the urethra cross section is star-shaped.[8] Gleason filmed the urethral opening of humans when volunteers voided on a portable commode. He showed that the cross section of the opening is elliptical.[9] Other experimental techniques are used to visualize the urethra when urine is flowing, including sonography,[10–12] x-ray,[13] computed tomography (CT) scan,[14] magnetic resonance,[15] and fluorescence imaging.[16] However, none of these techniques can depict the lumen in enough resolution to be used in modeling the flow.

Previous studies use histology to estimate the cross-sectional area of a dry urethra.[1] However, the cross-sectional area measured this way may be underestimated since the urinary flow expands the urethra. In humans, the coordinated engagement of the pelvic muscles prevents air from entering the reproductive tract during urination.[17] In our mathematical model, we assume that the reproductive tract is filled during urination. We use CT scan to measure the urethra of several mammals when they are filled with fluid to obtain a realistic shape profile.

Understanding the mechanics of micturition is still an open problem, although progress has been made with studies of human males and females as well as animal models. Males generally void using detrusor pressure, whereas females do so using a combination of detrusor pressure, abdominal pressure, or perineal relaxation with little or no pressure.[18–22] Recent work suggests that gravity plays a role in micturition across mammal species and causes the constant urination time of 21 s from dogs to elephants.[1] During the steady-state phase of micturition, driving forces are balanced by resisting forces. While driving forces have been studied using direct pressure measurement, the origins of the resisting forces are poorly understood. Many studies assume without explanation that viscous force is negligible.[1,18,21–25] However, it has been well known in engineering that the roughness on the inner walls of pipes resists flow. Such roughness increases fluid turbulence, and more pressure must overcome the accompanying viscous dissipation to push the fluid through the pipe. For many years, roughness is accounted for in modeling the flow of water, petroleum, and other liquids in rough pipes. The viscous losses in the urinary system are challenging to characterize since the lumen is soft and collapses on itself without the pressure of a flowing fluid. The goal of this study is to characterize the lumen roughness and to predict the urinary speed associated with these shapes.

This study investigates the influence of shape and roughness of urinary flow. In Section 2, we provide detailed methods. In Section 3, we report the visualization of the urethra, measurements of urethral roughness, experiments on three-dimensional (3D) printed urethral replicas, and the mathematical model for urination based on our measurements. In Section 4, we discuss our work's implications and suggest future research directions. In Section 5, we summarize the contributions of our study.

2 | MATERIALS AND METHODS

2.1 | μCT scan on urethras

We obtained access to six deceased animals that were leftover from other animal studies at Georgia, T3 Labs, and local farms. These specimens included three pigs, two rabbits, and one cat, as listed in Table 1. We used scalpels to carefully harvest the entire urinary system, which included the bladder and the urethra. We filled these urethras with a radiopaque silicon rubber compound and analyzed them by micro-CT (μCT) scan, capable of 43-μm resolution.

If the bladder contained urine, we sucked it out using a syringe. We flushed the insides of the tissue by injecting saline (0.9% sodium chloride) in the direction of urine flow. Afterward, we tied off the external orifice using a suture thread. We filled the urethra with Microfill solution (Microfill:diluent:catalyst = 5:5:1) to its maximum capacity using a syringe. After filling, we tied off the end of the bladder with suture thread and refrigerated the tissue in the saline solution overnight.

We scanned the urethra, as shown in the inset of Figure 1C, using a μCT 40 (Siemens Inveon) with an effective pixel size of 43 μm. We reconstruct the cross-sections and analyze the images using the software ImageJ. The urethra has irregular cross-sections, so we introduce the concept of hydraulic diameter used for a noncircular duct.[26] We measure the cross-sectional area

A and perimeter P with image analysis and then define the inner diameter D of the urethra as

$$D = \frac{4A}{P}. \quad (1)$$

From hereon, we refer to the diameter calculated from Equation (1).

2.2 | Urinary system replica

We 3D printed urethral replicas in 2-cm-long segments, with a diameter of $D = 4.9$ mm and an inner-wall roughness of $\varepsilon = 0.241$ mm. The diameter is estimated for a 10-kg dog by Equation (4). The replica was designed in Solidworks and then 3D printed with the Form 2 Stereolithography (SLA) printers using Formlabs Flexible FLGR02 resin on a 0.05 mm z-layer height setting to maximize resolution. We printed both smooth tubes and rough tubes. The smooth tubes were printed without any bumps, so the roughness was set by the resolution of the 3D printer. The rough tubes were printed with 0.241 mm hemispherical bumps lining the inside of the segments.

We connected the segments together to study the urethras of aspect ratios from 7 to 44. The segments adhered to the bottom of a yogurt container, which acts as a bladder. For each experiment, we filled the replica with water of $V = 300$ mL, and measured the emptying time T. The cross-section of the replica was $A = \pi D^2/4$; thus, the average speed of the flow was $u = V/AT$. For every 50 mL of volume released, we measured the average flow rate and speed of flow by measuring the released fluid's volume. We conducted 20 experiments by connecting segments of various lengths, allowing us to determine the relationship between urethra length and urinary speed.

3 | RESULTS

3.1 | Urethra geometry and roughness

We harvested six animal urinary systems, including three pigs, two rabbits, and one cat. We filled the urethras with radiopaque silicon rubber compound and imaged them with a μCT scan as described in Section 2.1 and Supporting Information: Video S1.

We observed two kinds of urethra: nozzle-shaped urethras for female mammals and pipe-shaped urethras for male mammals. Note that female humans and rats have pipe shaped urethras too, but those were not measured here. We discuss the two kinds of urethra in turn. We defined the distance traveled by urine as the urogenital length, L_{female}, the distance from the neck of the bladder to the orifice. Female pigs and female rabbits have nozzle-shaped urethras in which the urethra merges with a segment of the reproductive tract, as shown in Figure 2A–C and Supporting Information: Figure SI. Previous studies also report that female dogs[27] and female elephants[28] have urethras that merged with the reproductive tract. We compile the urogenital length for female animals with nozzle-shaped urethras, including rabbits, pigs, dogs,[27] and elephants,[28] as well as female rats and female humans with pipe-shaped urethras. The relationship between animal mass M and L_{female} is shown in Figure 2F, where the best fit is given by the red dashed line

$$L_{\text{female}} = 30M^{0.45} \quad (N = 41, R^2 = 0.94). \quad (2)$$

Male pigs have piped-shaped urethras, as shown in Figure 2D,E. The distance traveled by urine is the urethral length, L_{male}. We compile the urethral length for male animals in the previously reported list,[1] including guinea pigs, cats, humans, lions, and elephants. The relationship between animal mass M and L_{male} is shown in Figure 2F, where the best fit is given by the blue dashed line:

$$L_{\text{male}} = 56M^{0.34} \quad (N = 10, R^2 = 0.91). \quad (3)$$

As shown in Figure 2F, female urethras are shorter than male urethras. The sex difference is consistent with previous reports of dogs[29] and cats.[30] Note that the species can affect urethra anatomy. The female animals in this study have urethras connected to the reproductive tract, but female mice,[31] female rats,[32] and female humans[33] have their urethras and reproductive tracts completely separated.

Female animals in this study have nozzle-shaped urethra, where the distal end has a smaller diameter than the proximal end. In contrast, male pigs exhibit pipe-shaped urethra, as shown in Figure 2D,E. We used image analysis to measure the perimeter of the urethra and infer its hydraulic diameter, as described in Section 2.1. Figure 1B shows the diameter as a function of distance from the bladder. The influence of the shape of the urethra will be addressed in Section 4.

We defined inner diameter D as the average diameter measured across the length of the urethra. We combined this data with the geometries of the urethra previously reported.[7,34–41] The relationship between animal mass M and inner diameter D is shown in Figure 2G, where red circles are females and blue triangles are males. Male and female animals of similar size had comparable diameters.

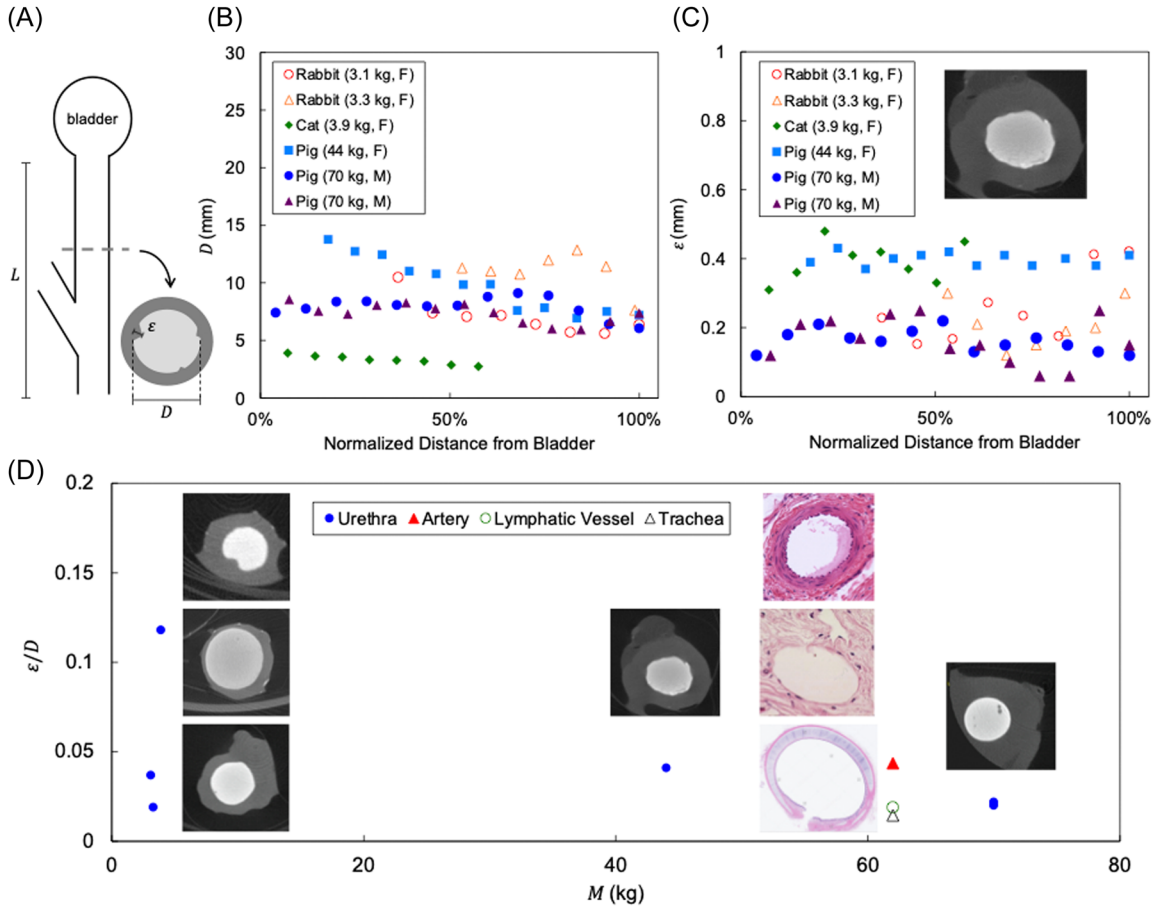

FIGURE 1 (A) Schematic of the urinary system for female pigs and rabbits. L is the distance traveled by urine, from the neck of the bladder to the urogenital opening. D is the inner diameter of the urethra. ε is the roughness of the urethral wall, which is the height of the tallest bump in the cross-sectional area. (B) The diameter of the urethra, D, and (C) the roughness of the urethral wall, ε, as functions of the normalized distance from the bladder. (D) The relationship between body mass M and the relative roughness of biological pipes ε/D.

Therefore, we used a single best fit across genders, as shown by the black dashed line. The best fit is

$$D = 2.2M^{0.37} \quad (N = 25, R^2 = 0.80), \tag{4}$$

where D is in millimeter and M is in kilogram. Equation (4) is comparable to the urethral diameter of $2M^{0.39}$ from our previous study.[1] Because our study is focused mostly on the influence of bumps, we idealize the urethra as a straight pipe similar to the male urethra. The aspect ratio of the urinary passage is defined as the ratio of urethra length to diameter, Ar= L/D. This aspect ratio depends on body size, but we take the average value across animals measured to be 14 for females and 25 for males. Thus, males have nearly double the urethra length of females.

Now that we have described the geometry of the urethra, we turn to the smaller-scale bumps visible on cross-sectional views, as shown in Figure 1A. To determine the height of the bump at various distances along the urethra, we identify by eye the tallest bump at each cross-section of the CT scan. Figure 1C shows the relationship between bump height ε and the distance from the bladder, normalized with urethral length. The roughness ranges from 0.1 to 0.4 mm as shown in Figure 1C, which is a small range compared to the 20-fold range in mass for the animals measured. The average roughness across all the mammals is

$$\varepsilon = 0.26 \pm 0.11\,\text{mm} \quad (N = 5), \tag{5}$$

and we use Equation (5) for the mathematical modeling and replica experiments

To compare the urethra roughness to other pipes in the body, we consider the relative roughness, ε/D, which is the roughness divided by the diameter of the urethra. Figure 1D shows the relative roughness of the six urethra samples compared to those of other biological pipes. For the urethra, relative roughness varies from 0.02 to 0.12 as shown in Table 1. These values are quite comparable to

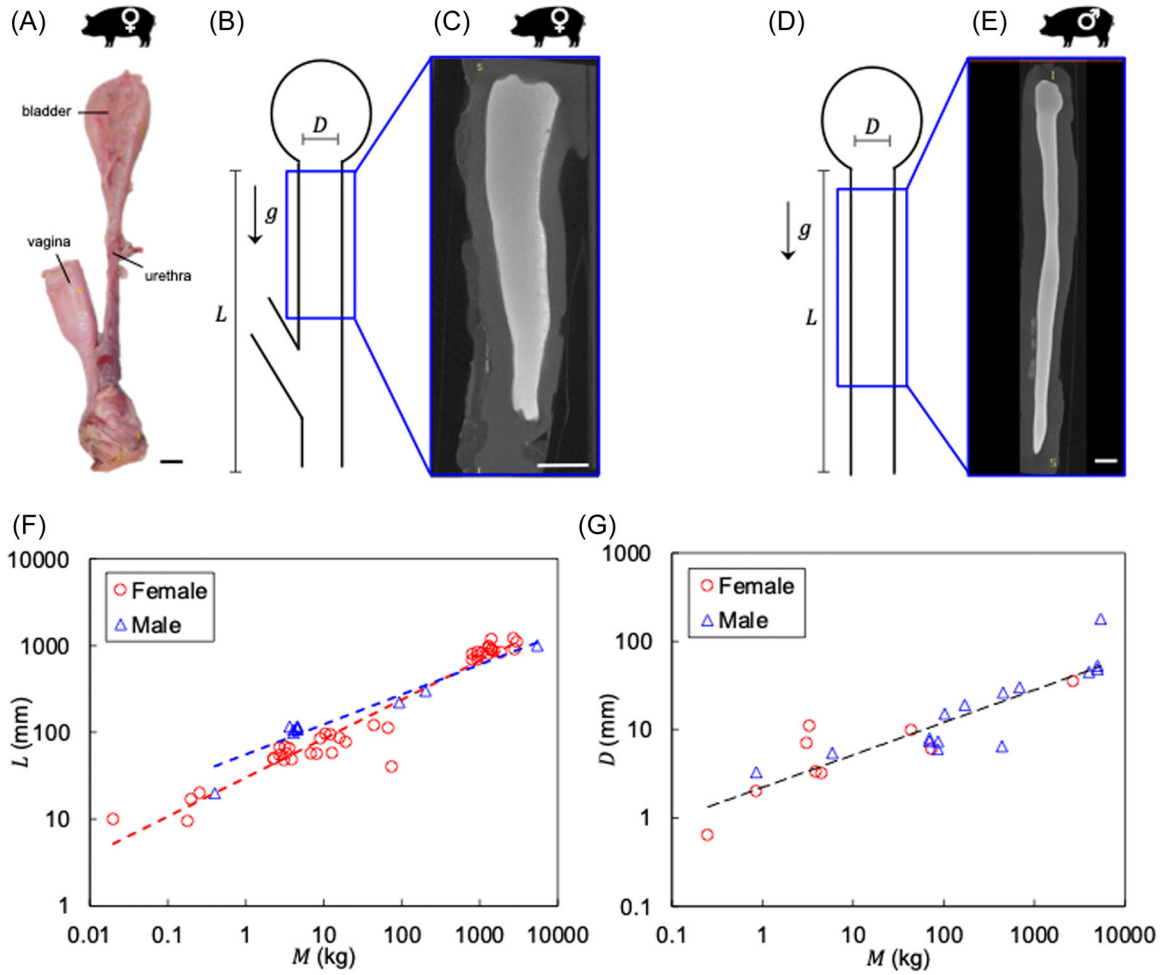

FIGURE 2 (A–C) The urinary system for female pigs and rabbits, where urine flows first through the urethra and then the reproductive tract. (D and E) The urinary system for male mammals, female rodents, and female humans, where urine flows through the urethra alone. (A) The urinary system dissected from a 44-kg female pig. Scale bar is 2 cm. (B) Schematic of the urinary system for female pigs and rabbits. *L* is the distance traveled by urine, from the neck of the bladder to the urogenital opening. *D* is the inner diameter of the urethra. (C) Micro-computed tomography (μCT) scan of a 44-kg female pig urethra. Scale bar is 1 cm. (D) Schematic of the urinary system for male mammals, female rodents, and female humans, where *L* is distance traveled by urine, from the neck of the bladder to the urogenital opening. *D* is the inner diameter of the urethra. (E) μCT scan of a 70-kg male pig urethra. Scale bar is 1 cm. (F and G) The relationship between body mass *M* and (F) the diameter of urethra *D*, and (G) the distance *L* traveled by urine. Symbols represent experimental measurements and dashed lines represent best fits to the data.

TABLE 1 μCT-scan measurement of urethras.

Animal	Sex	Body mass, *M* (kg)	Average inner diameter, *D* (mm)	Average roughness, *ε* (mm)	Relative roughness, *ε*/*D*
Rabbit	F	3.1	7.02	0.26	0.04
Rabbit	F	3.3	11.00	0.21	0.02
Cat	F	3.9	3.33	0.39	0.12
Pig	F	44	9.81	0.40	0.04
Pig	M	70	7.92	0.16	0.02
Pig	M	70	7.37	0.16	0.02

Abbreviations: F, female; M, male; μCT, micro-computed tomography.

those of human arteries ($\varepsilon/D = 0.04$),[42] lymphatic vessels ($\varepsilon/D = 0.02$),[43] and tracheae ($\varepsilon/D = 0.01$).[44] Moreover, we do not see any systematic trends in body mass. Now that we have quantified the geometry of the urethra, we use mathematical modeling to predict the effect of roughness on flow speed.

3.2 | Mathematical model

We present a mathematical model for the flow in the urethra that incorporates the roughness of the walls and thus goes one step further than our previous model.[1] We consider only gravity as the driving force, consistent with the experimental setup in Section 3.3; however, by following previous theoertical methods,[1] future workers may also account for bladder pressure. We assume the brief transient period is negligible and only consider the steady flow.[1] The urine is an incompressible fluid of density ρ and dynamic viscosity μ. At steady state, Newton's Law states that the forces balance: specifically, the gravitational force is balanced by inertia and viscous forces

$$P_{\text{gravity}} = P_{\text{inertia}} + P_{\text{viscosity}}. \tag{6}$$

Each term in Equation (6) is calculated as the pressure difference between the vertical pipe's entrance and exit. The hydrostatic pressure scales with the length of pipe: $P_{\text{gravity}} = \rho gL$, where g is the acceleration of gravity. Dynamic pressure $P_{\text{inertia}} = \rho u^2/2$is associated with the inertia of the flow, where u is the flow speed. The viscous pressure drop, also called major loss, in a long pipe is given by the Darcy–Weisbach equation[26]

$$P_{\text{viscosity}} = f_{\text{D}} \frac{\rho L u^2}{2D}. \tag{7}$$

The Darcy friction factor f_{D} is a function of the Reynolds number Re= $\rho uD/\mu$ and relative roughness ε/D, which is calculated by an online Moody chart solver.[45] For simplicity, we neglect the height of the water in our "bladder," in this case, a beverage container. Substituting these terms into Equation (5), we arrive at

$$\rho gL = \frac{\rho u^2}{2}\left(1 + f_{\text{D}} \frac{L}{D}\right). \tag{8}$$

Rearranging this equation in terms of the flow speed u yields

$$u = \sqrt{\frac{2gL}{1 + f_{\text{D}} \frac{L}{D}}}. \tag{9}$$

The urinary speed is a ratio of gravitational forces and viscous effects, which both scale with pipe length. As the urethra increases in length, the gravitational head is balanced by viscous forces. Thus, we expect a maximum urinary speed as the pipe length approaches infinity. We further calculate the speed when the aspect ratio of the pipe approaches infinity. We rewrite Equation (9) as a function of aspect ratio, Ar,

$$u = \sqrt{\frac{2gD\text{Ar}}{1 + f_{\text{D}}\text{Ar}}}. \tag{10}$$

We estimate the limits of u with L'Hospital's rule,

$$u_{\max} = \lim_{\text{Ar}\to\infty} u = \sqrt{\frac{2gD}{f_{\text{D}}}}. \tag{11}$$

Since this maximum speed is asymptotic, real urethras can never achieve it. Thus, we define the optimal aspect ratio of urethra, Ar*, as one that generates flow speeds of 80% of the maximum speed, $u/u_{\max} = 0.8$. Using Equations (10) and (11), we arrive at

$$0.8 = \sqrt{\frac{f_{\text{D}}\text{Ar}^*}{1 + f_{\text{D}}\text{Ar}^*}}. \tag{12}$$

The Darcy friction factor f_{D} is nearly independent of the aspect ratio of each replica in the regime of our experiments. With the average f_{D} of 0.08, the optimal aspect ratio Ar* is 22 in the urethra theoretically. Now we have the predicted optimal aspect ratio of the urethra, and we proceed with fabricating urethra replicas for flow testing.

3.3 | Experiments with urethral replicas

We design a replica of the urethra of a 10-kg male dog, which has $D = 4.9$ mm, $\varepsilon = 0.26$ mm, and aspect ratio Ar= 25, estimated from Equations (4) and (5). The bumps are hemispheres arranged in a square lattice, as shown in Figure 3C,D. We 3D-printed rough and smooth urethras, and we consider the smooth urethra as a control. The rough urethra had hemispherical bumps of 0.241 ± 0.037 mm ($N = 17$); the smooth one had a roughness that is an order of magnitude smaller, 0.026 ± 0.008 mm ($N = 5$), set by the resolution of the 3D printer.

We hypothesize that the flow speed varies with the aspect ratio of the urethra, as predicted by Equation (10). By 3D printed segments of the urethra, we create urethras that span aspect ratios from 7 to 44. Note that the biologically relevant urethra has an aspect ratio of

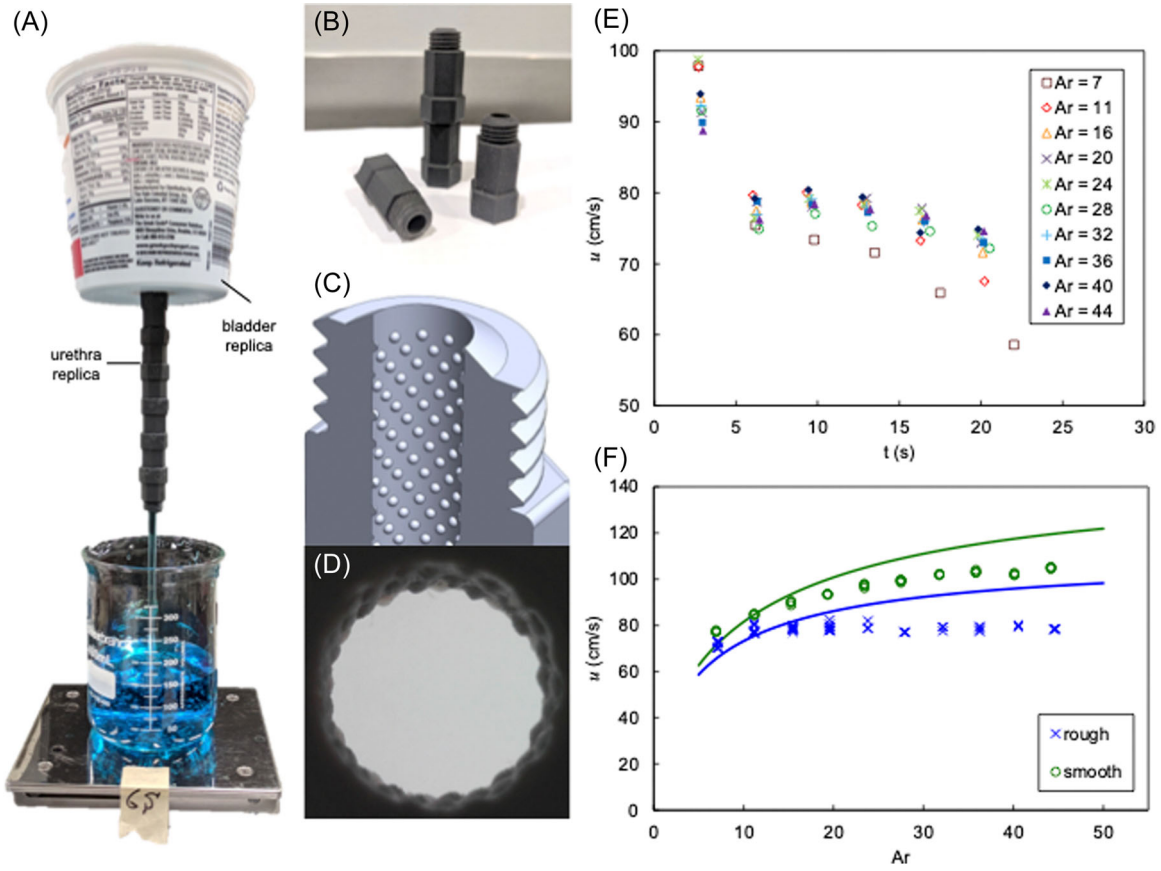

FIGURE 3 (A) Physical model of the urinary system with a rough lumen. (B) Three-dimensional (3D)-printed urethra with closeups of the lumen roughness. (C) Computer-aided design (CAD) model and (D) photograph. (E) Time course of the flow speed, u, through rough urethra replicas of varying aspect ratio, Ar. (f) Relationship between flow speed, u, and the aspect ratio of the urethra, Ar. Symbols represent experimental measurements and lines represent theoretical prediction.

Ar= 37 for 12-kg male dogs[46] and Ar= 14 for 9-kg female dogs.[47] Figure 3E shows the time course of the urinary speed. The speed becomes steady after 3 s, or equivalently, the first 50 mL or 16% of the volume is released. Although our system has no bladder pressure applied, it demonstrates a transient in urination, in analogy with human urinary systems, due to the filling of the urethra and acceleration of fluid within it from an initially empty state. From here on, we calculate the average urinary speed across the entire duration, including the transient period.

Figure 3F shows the relationship between the average urinary speed and the aspect ratio of the urethra replicas. Experiments are given by symbols, and prediction from Equation (10) is given by solid lines. For the rough urethra replicas ($\varepsilon = 0.241$ mm), the maximum speed is 78 cm/s, which is 25% less than that for smooth replicas ($\varepsilon = 0.026$ mm). For the smooth urethra, the urination speed reaches 85% of the maximum speed for aspect ratios greater than 7. Longer aspect ratios maintain the same diameter but increase the length. We see that such urethras do not lead to faster urination.

In agreement, our mathematical model also shows that aspect ratios do not eject urine faster. A longer urethra yields more gravitational energy but also suffers from more viscous dissipation. Mammals must maintain a constant aspect ratio if they wish to evolve to larger sizes: a male human has a urethra length of 240 mm, and a male elephant has a urethra length of 1000 mm. This range of sizes is only possible because mammals maintain a constant aspect ratio (for male animals, Ar= 25), which changes the surface-to-volume ratio of the urethra and permits faster urination speeds.

The model is a good match to the experiments for low aspect ratios but decreases in accuracy for high aspect ratios. The maximum speed of 146 and 110 cm/s by Equation (10) is 40% higher than 104 and 78 cm/s in the experiment. Our theory predicts an asymptotic trend that matches qualitatively with the trend for the smooth urethra. However, experiments with the rough urethra are not clearly asymptotic: instead, maximum values are

reached for only an aspect ratio of 10 and then fluctuate thereafter. The fluctuation might be due to fluid mechanical effects in rough channels. More in-depth fluid mechanical considerations show the frictional force increases with the aspect ratio of the rough channel.[48]

We compare the accuracy of both the replica experiment and the mathematical model to the urinary speed of a 10-kg male dog, which has a urethra length of 122 mm and a diameter of 5 mm by Equations (3) and (4). As reported previously,[1] a 10-kg male dog has a urination flow rate of $Q_M \approx 3$ mL/s. If we assume negligible contribution of the bumps, the urethra cross-sectional area is $A = \pi D^2/4 \approx 0.2\,\text{cm}^2$. Using the urinary speed at Ar= 25, the replica experiment and the mathematical model yield a flow rate of 24 and 18 mL/s, which are at least 6-fold faster than the reported value.[1]

4 | DISCUSSION

Our main contribution to this study is the measurement of the urethra lumen roughness and the incorporation of this roughness into the mathematical model and replica experiments. Despite this extra effort, our models still have six times greater flow rates than the reported value. Here, we bring up possible reasons for this discrepancy.

In our model, we assumed that the urethra has a constant diameter, but for many female mammals, we found the urethra was tapered, whose consequences we discuss here. A wider urethra–bladder connection has been reported for mice,[31] dogs,[29] cats,[30] and humans.[33] Previous researchers have hypothesized that the microfolds on the urethra lumen adhere bacteria, which may remain and even flow back into the bladder and cause infection.[49] Upstream contamination is also found in other contexts, such as tea preparation.[50] The tea leaves in a cup flow upward to the pot when the hot water spout is close to the leaves. A nozzle shape of the urethras increases the distal flow rate and the shear force, which may help wash out bacteria.

Since natural urine flow rates are faster than in our urethra replicas values, we conclude that our 3D-printed lumen and do not adequately capture the flow resistance. In our study, we completely inflated the urethra with radiopaque material, but in vivo, the soft urethra might be only partially distended with urine, which changes its resistance. Furthermore, we replicated the soft urethra using rigid 3D-printed materials, but in vivo, the bumps in the soft urethra may be deformed by the urinary flow. To determine the actual shape of the urethra during urination, visualization of the lumen in vivo would require noninvasive techniques, including sonography and x-ray with a resolution of around 40 μm.

Our model does not include bladder and abdominal pressures, which drive urinary flow. The maximum pressure of the bladder is 5.2 kPa across mammal species.[1] However, bladder pressure depends on bladder fullness during voiding, generating u-shaped time courses for bladder pressure.[5] The u-shaped time course of pressure causes the urinary flow to be unsteady over the voiding time. The gravitational-driven flow in our study does not have those dynamics, but future modeling might take them into account.

What is the origin of the roughness in the urethras? The urethral roughness is 200 times the roughness of polyvinyl chloride pipes used in modern plumbing. This is because biological pipes can only be as smooth as their constituent cells, which have volume independent of body size.[31] While we did not use microscopes to examine the bumps in the lumen, their characteristic size of 0.1 mm is comparable to the diameter of the largest human cell, the egg cell.

5 | CONCLUSION

In this study, we used experimental and theoretical methods to understand how urinary flow is affected by the roughness of the lumen. We presented an experimental method to inflate mammal urethras and measure their shape with a CT scanner. We used these measurements to design and 3D printed urethral replicas with the same roughness as those observed. We also presented a theoretical model for the urinary flow speed considering the roughness observed. Urinary flow speeds increased with aspect ratio, but with diminishing returns in a smooth urethra replica, and with fluctuations in a rough replica. Our replicate experiments generate speeds that are 40% slower than our mathematical models. Dog urination speeds are 6-fold faster than in our replica, indicating that there is still much to be understood in how the urethra resists flow.

AUTHOR CONTRIBUTIONS

Patricia J. Yang and David L. Hu contributed to the conception or design of the work. Patricia J. Yang, Tony G. Chen, Sarah B. Bracher, Aaron Hui, and David L. Hu contributed to the acquisition, analysis, or interpretation of data. Patricia J. Yang and David L. Hu have drafted the work and revised it.

ACKNOWLEDGMENTS

We acknowledge our hosts at animal facilities at Georgia Tech (L. O'Farrell) and T3 Labs (R. Bradley). We thank S. Jung for the discussions, A. Lin for her support in using the μCT scan, and M. LaMarca and J. Chang for their

early contributions. The study is supported by our funding sources: National Science Foundation Faculty Early Career Development Program (Division of Physics) Grant No. 1255127, Yushan Fellow Program by the Ministry of Education (MOE), Taiwan, and Georgia Tech Presidents Undergraduate Research Awards.

CONFLICT OF INTEREST STATEMENT

The authors declare no conflict of interest.

DATA AVAILABILITY STATEMENT

The data that support the findings of this study are available from the corresponding author upon reasonable request.

ORCID

Patricia J. Yang http://orcid.org/0000-0002-9274-7042
David L. Hu http://orcid.org/0000-0002-0017-7303

REFERENCES

1. Yang PJ, Pham J, Choo J, Hu DL. Duration of urination does not change with body size. *Proc Natl Acad Sci USA*. 2014;111:11932-11937.
2. Kim K-W, Park S-H, Im G, et al. CFD study on vesicoureteral reflux in the urinary tract with double J stent. *Comput Biol Med*. 2022;145:105456.
3. Batzegari M, Vahidi B, Safarinejad MR, Ebad M. A computational analysis of the effect of supporting organs on predicted vesical pressure in stress urinary incontinence. *Med Biol Eng Comput*. 2020;58:1079-1089.
4. Trostorf R, Morales Orcajo E, Pötzke A, Siebert T, Böl M. A pilot study on active and passive ex vivo characterisation of the urinary bladder and its impact on three-dimensional modelling. *J Mech Behav Biomed Mater*. 2022;133:105347.
5. Jaskowak D, Nunez R, Ramachandran R, et al. Mathematical modeling of the lower urinary tract: a review. *Neurourol Urodyn*. 2022;41:1305-1315.
6. Takanashi A, Sakai-Saito A, Hattori T, Kanno-Saito S, Katano Y, Okada T. Differences between young and aged rats in voiding frequency and detrusor muscle serotonergic contraction. *Exp Gerontol*. 2019;124:110642.
7. Gray H. *Anatomy of the Human Body*. Lea & Febiger; 1918.
8. Woodburne RT, Lapides J. The ureteral lumen during peristalsis. *Am J Anat*. 1972;133:255-258.
9. Gleason DM, Bottaccini MR, Reilly RJ. The shape and cross-sectional area of the distal urethra critically affects urinary flow. *Invest Urol*. 1971;8:585-595.
10. Prasad SR, Menias CO, Narra VR, et al. Cross-sectional imaging of the female urethra: technique and results. *Radiographics*. 2005;25:749-761.
11. Ishii T, Yiu BYS, Yu ACH. Vector flow visualization of urinary flow dynamics in a bladder outlet obstruction model. *Ultrasound Med Biol*. 2017;43:2601-2610.
12. Ishii T, Nahas H, Yiu BYS, Chee AJY, Yu ACH. Contrast-enhanced urodynamic vector projectile imaging (CE-UroVPI) for urethral voiding visualization: principles and phantom studies. *Urology*. 2020;140:171-177.
13. Fonda D, Hickey DS, Brocklehurst JC. Dynamic shape of the female urethra during micturition. Clinical methods. *J Urol*. 1985;134:88-91.
14. Pullan BR, Phillips JI, Hickey DS. Urethral lumen cross-sectional shape: its radiological determination and relationship to function. *Br J Urol*. 1982;54:399-407.
15. Shimatani K, Soufi M, Sato Y, Yamamoto S, Kanematsu A. Why upright standing men urinate more efficiently than in supine position: a morphological analysis with real-time magnetic resonance imaging. *Neurourol Urodyn*. 2022;41:1074-1081.
16. Al-Taher M, Knapen B, Barberio M, et al. Near infrared fluorescence imaging of the urethra: a systematic review of the literature. *Minim Invasive Ther Allied Technol*. 2022;31(3):342-349.
17. Kent T, Northrup C, Northrup K. *Mothering from Your Center: Tapping Your Body's Natural Energy for Pregnancy, Birth, and Parenting*. Atria Books/Beyond Words; 2013.
18. Rao SG, Walter JS, Jamnia A, Wheeler JS, Damaser MS. Predicting urethral area from video-urodynamics in women with voiding dysfunction. *Neurourol Urodyn*. 2003;22:277-283.
19. Barnea O, Gillon G. Model-based estimation of male urethral resistance and elasticity using pressure–flow data. *Comput Biol Med*. 2001;31:27-40.
20. Walter JS, Wheeler JS, Morgan C, Plishka M. Urodynamic evaluation of urethral opening area in females with stress incontinence. *Int Urogynecol J*. 1993;4:335-341.
21. Gleason DM, Bottaccini MR. The vital role of the distal urethral segment in the control of urinary flow rate. *J Urol*. 1968;100:167-170.
22. Gleason DM, Bottaccini MR, Perling D, Lattimer JK. A challenge to current urodynamic thought. *J Urol*. 1967;97:935-940.
23. Tziannaros M, Glavin SE, Smith FT. Three-dimensional effects in the lower urinary tract. *IMA J Appl Math*. 2013;78:729-749.
24. Jang K-S, Kim J-W, Ryu J. Numerical investigation of urethra flow characteristics in benign prostatic hyperplasia. *Comput Methods Programs Biomed*. 2022;224:106978.
25. Cohen AJ, Baradaran N, Mena J, Krsmanovich D, Breyer BN. Computational fluid dynamic modeling of urethral strictures. *J Urol*. 2019;202:347-353.
26. Munson BR, Young DF, Okiishi TH. *Fundamentals of Fluid Mechanics*. Wiley; 1990.
27. Johnston GR, Osborne CA, Jessen CR. Effects of urinary bladder distension on the length of the dog and cat urethra. *Am J Vet Res*. 1985;46(2):509-512.
28. Balke JME, Boever WJ, Ellersieck MR, Seal US, Smith DA. Anatomy of the reproductive tract of the female African elephant (*Loxodonta africana*) with reference to development of techniques for artificial breeding. *Reproduction*. 1988;84:485-492.
29. Cullen WC, Fletcher TF, Bradley WE. Histology of the canine urethra. I. Morphometry of the female urethra. *Anat Rec*. 1981;199:177-186.

30. Cullen WC, Fletcher TF, Bradley WF. Morphometry of the female feline urethra. *J Urol*. 1983;129:190-192.
31. Phillips JI, Davies I. A comparative morphometric analysis of the component tissues of the urethra in young and old female c57bl/icrfat mice. *Invest Urol*. 1981;18:422-425.
32. Chang S-C, Chern I, Bown SG. Photodynamic therapy of rat bladder and urethra: evaluation of urinary and reproductive function after inducing protoporphyrin IX with 5-aminolaevulinic acid. *BJU Int*. 2000;85:747-753.
33. Carlile A, Davies I, Rigby A, Brocklehurst JC. Age changes in the human female urethra: a morphometric study. *J Urol*. 1988;139:532-535.
34. Souza ABGd, Suaid HJ, Suaid CA, Tucci Jr. S, Cologna AJ, Martins ACP. Comparison of two experimental models of urodynamic evaluation in female rats. *Acta Cir Bras*. 2008;23:59-65.
35. Root MV, Johnston SD, Johnston GR, Olson PN. The effect of prepuberal and postpuberal gonadectomy on penile extrusion and urethral diameter in the domestic cat. *Vet Radiol Ultrasound*. 1996;37:363-366.
36. Hildebrandt TB, Goritz F, Pratt NC, et al. Ultrasonography of the urogenital tract in elephants (*Loxodonta africana* and *Elephas maximus*): an important tool for assessing female reproductive function. *Zoo Biol*. 2000;19:321-332.
37. Tsujimoto Y, Nose Y, Ohba K. Experimental and clinical trial of measuring urinary velocity with the pitot tube and a transrectal ultrasound guided video urodynamic system. *Int J Urol*. 2003;10:30-35.
38. Pozor MA, McDonnell SM. Ultrasonographic measurements of accessory sex glands, ampullae, and urethra of normal stallions of various size types. *Theriogenology*. 2002;58:1425-1433.
39. Bailey CB. Siliceous urinary calculi in bulls, steers, and partial castrates. *Can J Anim Sci*. 1975;55:187-191.
40. Hildebrandt TB, Göritz F, Pratt NC, et al. Reproductive assessment of male elephants (*Loxodonta africana* and *Elephas maximus*) by ultrasonography. *J Zoo Wildlife Med*. 1998;29:114-128.
41. Fowler ME, Mikota SK. *Biology, Medicine, and Surgery of Elephants*. Wiley; 2008.
42. Spitalnik PF. *Blood Vessels. Histology Laboratory Manual 2016-2017*. Columbia University; 2016.
43. Friedlander E. *Dilated Lymphatic Vessel*. Ed's Basic Histology Gallery; 2010.
44. Transverse (cross sectional) view of the trachea (wind pipe) showing the circular cartilage (gray-light blue) and epithelial lining. vetpathologist. Accessed 2018. https://www.shutterstock.com/image-photo/transverse-cross-sectional-view-trachea-wind-90521116
45. Cimbala JM. *Moody Chart Solver*. https://www.me.psu.edu/cimbala/me325web_Spring_2012/Excel/Moody_chart_solver.xls.
46. Kang K, Kim K, Oh D, Choi J, Choi M, Yoon J. Retrograde CT urethrography using a power injector quantitatively reveals effects of bladder distension on urethral size in healthy male Beagle dogs. *Vet Radiol Ultrasound*. 2020;61:302-311.
47. Kang K, Kim K, So J, et al. The urethra of healthy female dogs can be normally narrowed due to the urethral flexure in retrograde CT urethrography. *Vet Radiol Ultrasound*. 2021;62:61-67.
48. Wagner RN, Kandlikar SG. Effects of structured roughness on fluid flow at the microscale level. *Heat Transfer Eng*. 2012;33(6):483-493.
49. Hinman Jr., F. Hydrodynamic aspects of urinary tract infection. *Urodynamics: Upper and Lower Urinary Tract*. 1973:14-22.
50. Bianchini S, Lage A, Siu T, Shinbrot T, Altshuler E. Upstream contamination by floating particles. *Proc R Soc Ser A*. 2013;469:20130067.

SUPPORTING INFORMATION

Additional supporting information can be found online in the Supporting Information section at the end of this article.

How to cite this article: Yang PJ, Chen TG, Bracher SB, Hui A, Hu DL. Urinary flow through urethras with a rough lumen. *Neurourol Urodyn*. 2023;42:1245-1254. doi:10.1002/nau.25186